Development of a balloon-borne instrument for CO_2 vertical profile observations in the troposphere

Mai Ouchi[1], Yutaka Matsumi[1*], Tomoki Nakayama[2], Kensaku Shimizu[3], Takehiko Sawada[3], Toshinobu Machida[4], Hidekazu Matsueda[5], Yousuke Sawa[5], Isamu Morino[4], Osamu Uchino[4], Tomoaki Tanaka[6,a], Ryoichi Imasu[7]

[1]Institute for Space-Earth Environmental Research and Graduate School of Science, Nagoya University, Furo-cho, Chikusa-ku, Nagoya, Aichi 464-8601, Japan

[2]Graduate School of Fisheries and Environmental Sciences, Nagasaki University, 1-14, Bunkyo-machi, Nagasaki, Nagasaki 852-8521 Japan

[3]Meisei Electric Co., Ltd., 2223 Naganumamachi, Isesaki, Gunma 372-8585, Japan

[4]National Institute for Environmental Studies, 16-2 Onogawa, Tsukuba, Ibaraki 305-8506 Japan

[5]Meteorological Research Institute, Japan Meteorological Agency, 1-1 Nagamine, Tsukuba, Ibaraki 305-0052, Japan

[6]Japan Aerospace Exploration Agency Earth Observation Research Center, 2-1-1, Sengen, Tsukuba, Ibaraki 305-8505, Japan

[7]Atmosphere and Ocean Research Institute, The University of Tokyo, 5-1-5, Kashiwanoha, Kashiwa, Chiba 277-8568, Japan

[a]now at: NASA Ames Research Center, Moffett Field Mountain View CA 94035, USA

Corresponding author: matsumi@nagoya-u.jp

Abstract

A novel, practical observation system for measuring tropospheric carbon dioxide (CO_2) concentrations using a non-dispersive infrared analyzer carried by a small helium-filled balloon (CO_2 sonde), has been developed for the first time. Vertical profiles of atmospheric CO_2 can be measured with a 240-400 m altitude resolution through regular onboard calibrations using two different CO_2 standard gases. The standard deviations (1σ) of the measured mole fractions in the laboratory experiments using a vacuum chamber at a temperature of 298 K were approximately 0.6 ppm at 1010 hPa and 1.2 ppm at 250 hPa. Two CO_2 vertical profile data obtained using the CO_2 sondes, which were launched on January 31st and February 3rd, 2011 at Moriya, were compared with the chartered aircraft data on the same days and the commercial aircraft data obtained by the Comprehensive Observation Network for TRace gases by Airliner (COTRAIL) program on the same day (January 31rd) and one day before (February 2nd). The difference between the CO_2 sonde data and these four sets of *in-situ* aircraft data (over the range of each balloon altitude ± 100 m) up to the altitude of 7 km was 0.6±1.2 ppm (average ± 1σ). In field experiments, the CO_2 sonde detected an increase in CO_2 concentration in an urban area and a decrease in a forested area near the surface. The CO_2 sonde was shown to be a useful instrument for observing and monitoring the vertical profiles of CO_2 concentration in the troposphere.

1. Introduction

Atmospheric carbon dioxide (CO_2) is one of the most important anthropogenic greenhouse gases for global warming. Certain human activities, such as fossil fuel combustion, cement production, and deforestation are the major cause of atmospheric CO_2, making the global average concentration of atmospheric CO_2 to increase from 280 ppm before the Industrial Revolution to 400.0 ppm in 2015 (World Meteorological Organization, WMO 2016). Over the last 10 years, the average rate of atmospheric CO_2 increase is measured at 2.21 ppm yr^{-1} (WMO 2016). Atmospheric CO_2 is measured by ground-based stations and ships using the flask sampling and continuous instrument methods such as non-dispersive infrared absorption (NDIR) (Tanaka et al. 1983, Hodgkinson et al. 2013) and cavity ring-down spectroscopy (CRDS) (Winderlich et al. 2010). A network of ground-based Fourier transforms spectrometers (FTS), that record the direct solar spectra in the near-infrared spectral region (Total Carbon Column Observing Network, TCCON), is used to observe the column-averaged mole fraction of CO_2 in dry air (total column XCO_2) (Wunch et al. 2011). These observations have provided extensive information, regarding the distribution and temporal variation of CO_2 in the atmosphere (Pales and Keeling, 1965; Conway et al. 1988; Komhyr et al. 1989; Tans et al. 1989; Conway et al. 1994). Moreover, atmospheric CO_2 measurements data are useful for estimating CO_2 fluxes at the surface through inverse modeling (Gurney et al. 2004; Baker et al. 2006). Due to the limited number of observation sites and the limitations of their altitudinal range, a large degree of uncertainty in the current estimates of the regional CO_2 sources and sinks is noted (Gurney et al. 2002). More atmospheric CO_2 measurements are needed to reduce the uncertainties in CO_2 fluxes estimation using an inverse modeling.

To address the issues with insufficient CO_2 observational data, satellite remote sensing techniques have been used to investigate the CO_2 distribution on a global scale (Chédin et al. 2002; Crevoisier et al. 2004; Dils et al. 2006). The Greenhouse Gases Observing SATellite (GOSAT), which measures the short wavelength infrared (SWIR) spectra of sunlight reflected by the earth's surface with a Fourier

transform spectrometer and obtains the total column XCO_2, has been in operation since early 2009 (Yokota et al. 2009; Yoshida et al. 2011; Morino et al. 2011). Since 2014, the Orbiting Carbon Observatory-2 (OCO-2) satellite has also measured the IR spectra of the surface reflected sunlight with a diffraction grating spectrometer and obtains total column XCO_2 (Eldering et al. 2017). However, these satellite observations provide only nadir total column XCO_2, and do not measure the vertical distributions of CO_2 concentrations, as the observed spectra of the surface-reflected sunlight do not provide enough information to determine the vertical distributions. Furthermore, the satellites overpass a specific earth-based target once several days only at about noon in the solar time because of their sun-synchronous orbits.

The altitude distributions of CO_2 concentrations have been measured using other techniques. For instance, tall towers measure vertical profiles of CO_2 near the ground (Bakwin et al. 1992, Inoue and Matsueda, 2001; Andrews et al. 2014). CO_2 vertical profiles up to 10 km near the airports have been observed by the equipment installed by the commercial airlines, such as the Comprehensive Observation Network for TRace gases by Airliner (CONTRAIL program) (Machida et al. 2008; Matsueda et al. 2008). Measurements by equipment installed on chartered aircrafts have also been undertaken, which include the High-performance Instrumented Airborne Platform for Environmental Research (HIAPER), Pole-to-Pole Observations (HIPPO) program up to 14 km in the altitude spanning the Pacific from 85° N to 67° S (Wofsy et al. 2011), the NIES/JAXA (National Institute of Environmental Studies and Japan Aerospace eXploration Agency) program at an altitude from 2 to 7 km (Tanaka et al. 2012), and the NOAA/ESRL Global Greenhouse Gas Reference Network Aircraft Program (Sweeney et al. 2015). Although these aircraft measurements provided the vertical profiles of CO_2 concentrations, vertical profile measurements using the commercial airlines are limited around the large airports and frequency of the measurements using chartered airplane is often limited by their relatively high cost. The continuation and expansion of airborne measurement programs for CO_2 and related tracers are expected to enhance the estimation of the global carbon cycling greatly (Stephens

et al., 2007).

Atmospheric CO_2 observations using balloons, to select specific locations unless prohibited or restricted by aircraft flight paths, are useful for solving the issues associated with the sparseness of CO_2 vertical data. Balloon-borne observations of stratospheric CO_2 are previously conducted by other studies. For instance, stratospheric air sampling was conducted using cryogenic sampler onboard balloons once a year from 1985 to 1995 over the northern part of Japan (Nakazawa et al. 1995). Balloon-borne near-infrared tunable diode laser spectrometers have been developed to provide in situ data for CO_2 in the stratospheric atmosphere (Durry et al. 2004; Joly et al. 2007, Ghysels et al. 2012). Furthermore, two in situ CO_2 analyzers adopting the NDIR technique, using a modified commercial detector for stratospheric measurements, have been developed for deployment on the NASA ER-2 aircraft and on a balloon (Daube et al. 2002). These balloon borne instruments described above were specially designed to measure CO_2 concentrations in the stratosphere.

Observation of the CO_2 vertical distribution in the troposphere is essential because the uncertainties in the estimated fluxes, using the inverse method, can be attributed to the inaccurate representations of the atmospheric processes in transport models. Misrepresentation of vertical mixing by the transport models, particularly inside of the boundary layer, which is the layer closest to the ground where CO_2 is taken up and released, is one of the dominant causes of the uncertainty in CO_2 flux estimation (Stephens et al. 2007; Ahmadov et al. 2009). Recently, the observation of tropospheric CO_2 was conducted, using a lightweight unmanned aerial vehicle, such as a kite plane, with a commercial NDIR instrument. CO_2 profiles were observed in and above the planetary boundary layer up to 2 km to investigate the temporal and spatial variations of CO_2 (Watai et al. 2006). A passive air sampling system for atmospheric CO_2 measurements, using a 150 m long stainless-steel tube called an AirCore was developed (Karion et al. 2010). The AirCore mounted on an airplane or a balloon ascends with evacuating inside of the tube to a high altitude of 30 km at flight maximum, then, collecting ambient air by pressure changes along a decrease in altitude. The sampled air in the tube is analyzed with the

118 precision of 0.07 ppm for CO_2 indicated as one standard deviation in the laboratory and the vertical
119 profile of CO_2 is obtained.

120 In the present study, we have developed a practical CO_2 sonde system that can measure in situ CO_2
121 vertical profiles in the atmosphere from the ground to altitudes up to about 10 km with a 240–400 m
122 altitude resolution by using a small-sized balloon. Although the sonde system is thrown away after
123 every flight due to the difficulties associated with recovery, the sonde systems are easily prepared with
124 a relatively low cost. We have tested the sonde flight experiments more than 20 times in Japan. The
125 CO_2 sonde developed has the following advantages, compared with other measurement techniques
126 described above: (1) its cost of operation is low and the flight permission is easy to obtain from the
127 authorities as compared with the aircraft observations; (2) the CO_2 sonde can be easily carried to the
128 launch sites since the instrument is light; (3) a limited amount of power is required for the operation;
129 (4) it can generally be launched at any time; and (5) the meteorological data are obtained
130 simultaneously with CO_2 profile data. In this study, the design of our novel CO_2 sonde and the results
131 of the comparison experiments with aircraft measurements are described. The target accuracy and
132 precision in the measurements with the CO_2 sonde are below about 1 ppm CO_2 mole fraction in the
133 atmosphere of 400 ppm CO_2, preferable for carbon cycle studies (e.g. Maksyutov et al. 2008). The
134 developed CO_2 sonde system attained virtually all the targets from the ground to an altitude of about
135 10 km.

136 Inai et al. (2018) measured vertical profiles of CO_2 mole fraction in the equatorial eastern and
137 western Pacific in February 2012 and February–March 2015, respectively, by using our novel CO_2
138 sondes which are described in this report. They found that the 1–10 km vertically averaged CO_2 mole
139 fractions lie between the background surface values in the Northern Hemisphere (NH) and those in the
140 Southern Hemisphere (SH) monitored at ground-based sites during these periods. Their study showed
141 that the combination of CO_2 sonde measurements and trajectory analysis, taking account of convective
142 mixing, was a useful tool in investigating CO_2 transport processes.

2. Materials and methods

a. Design of the CO_2 sonde

Many severe restrictions are noted for the operation of balloon-borne CO_2 sondes. First, the weight of the CO_2 sonde package should be less than about 2 kg, based on the legal restriction by the US FAA (Federal Aviation Administration) and by the Japanese aviation laws for the payload weight of 2.721 kg for unmanned free balloons. Balloon systems heavier than the above regulation weight are not useful for the frequent flights because the flight permission from the authorities is much more difficult to obtain, and the additional safety requirements are more expensive. The balloon system is thrown away in the ocean after each flight due to a long-distance transportation (100 km or more to the east) by strong westerly winds in the upper atmosphere of mid-latitude area. This is done to avoid the accidents associated with a falling onto the urban areas, resulting in high recovery costs. Therefore, the cost of the CO_2 sonde system should be low for frequent observations. The non-recovery system implies that every instrument should perform consistently.

In this study the NDIR technique was adopted for a detection of CO_2 concentrations. The NDIR CO_2 measurement techniques have been widely used in many places such as WMO/GAW (Global Atmosphere Watch) stations. Our target instrumental accuracy and precision of approximately 1 ppm are less stringent than those of the ground-based instruments (± 0.1 ppm) used at the WMO/GAW stations (WMO, 2016). However, the surrounding conditions for the instrument are substantially severe during the flight experiments, as the pressure changes from 1,000 to 250 hPa and the surrounding temperature changes from 300 to 220 K during flights from the surface to an altitude of 10 km in about 60 min.

In the NDIR technique for CO_2 measurements, the IR emission from a broadband wavelength source is passed through an optical cell and two filters, and then the light intensities are detected by two IR detectors. The one optical filter covers the whole absorption band of CO_2 around 4.3 μm, while the

other covers a neighboring non-absorbed region around 4.0 μm. provided that the chosen active and reference channel filters do not significantly overlap with the absorption bands of other gas species present in the application. (Hodgkinson et al., 2013).

The Beer–Lambert Law is expressed by Eq. (1), defining the light intensity in the absence of CO_2 in the cell as I_0 and the light intensity in the presence of CO_2 in the cell as I,

$$\frac{I}{I_0} = \exp(-\varepsilon C L) \qquad (1),$$

where C is the CO_2 concentration in molecules cm^{-3}, L is the optical path length in cm, and ε is the absorption cross-section in cm^2 $molecule^{-1}$. Using the relationship of $C = XP\,(k_B T)^{-1}$, where X is the CO_2 mole fraction and P is the pressure of dehumidified ambient air, and the approximation of $\exp(-\varepsilon C L) = 1 - \varepsilon C L$, under the condition of $\varepsilon C L << 1$, Eq. (1) is rewritten as:

$$\frac{(I_0 - I)}{P} = X \frac{I_0 \varepsilon L}{k_B T_C} \qquad (2),$$

where T_c is the sample air temperature in the sensor cell and k_B is the Boltzmann constant. The eq. (1) and (2) hold for monochromatic light only and that eq. (2) only holds for small absorptions. Although the NDIR analyzer exhibits non-liner absorption due to the saturation of strong absorption lines, the NDIR analyzer is known to have a good linearity within a certain concentration range (Galais et al. 1985). In our analyses of the balloon data, eq. (2) was used only for the interpolation between the low and high mole fractions of the in-flight calibration gases to obtain the ambient CO_2 mole fractions. With a 120 mm long absorption cell, the absorption intensity is approximately 3% at 400 ppm CO_2 with our CO_2 NDIR system, i.e., $\varepsilon CL \approx 0.03$ and the approximation of $\exp(-\varepsilon C L) = 1 - \varepsilon C L$ are well fitted. The values of $[I(4.0) - I(4.3)]$ were used instead of $(I_0 - I)$ to obtain the CO_2 mole fraction values in the NDIR measurements, where $I(4.0)$ and $I(4.3)$ were the signal intensities at the 4.0 μm wavelength for background measurements and the 4.3 μm wavelength for CO_2 absorption measurements, respectively. Thus, the value of $[I(4.0) - I(4.3)]/P$ is thus proportional to the CO_2

mole fraction X in the optical cell. The proportionality constant is usually determined by the measurements of the standard gases. In the NDIR measurements at the ground WMO/GAW stations, carbon dioxide mole fractions are referenced to a high working standard and a low working standard and are determined by the interpolations of the signals with the two standards, and the calibration with the two standard gases are carried out every 12 h (Fang et al., 2014).

b. System configuration of the CO_2 sonde system

A schematic diagram and photograph of the CO_2 measurement instrument are shown in Fig. **1**. The CO_2 sonde has three inlets installed for ambient air and two calibration gases with mesh filters (EMD Millipore, Millex-HA, 0.45 μm pore size) to remove the atmospheric particles. Three solenoid valves (Koganei, G010LE1-21) were used to switch the gas flow to the CO_2 sensor. A constant-volume piston pump with a flow rate of 300 cm^3 min^{-1} (Meisei Electric co., Ltd.), which is originally used for ozonesonde instruments, directed the gas flows from the inlets through the solenoid valves into a dehumidifier, a flow meter, and a CO_2 sensor. The absolute STP (standard temperature and pressure) flowrate decreased with a decrease in pressure. Since the exit port of the CO_2 sensor was opened to the ambient air, the pressure of dehumidified outside air and calibration gases in the absorption cell were equal to the ambient pressure during the flight. Next to the pump, the gases were introduced to a glass tube filled with the magnesium perchlorate grains (dehumidifier) installed upstream to the CO_2 sensor to remove the water vapor. Fabric filters were installed on both ends of the dehumidifier, and a mesh filter was installed downstream of the dehumidifier to prevent the CO_2 sensor from the incursion of magnesium perchlorate grains to the optical cell.

The infrared absorption cell consisted of a gold-coated glass tube, a light source, and a photodetector. The light source (Helioworks, EP3963) consisted of a tungsten filament with a spectral peak intensity wavelength of approximately 4 μm. The light from the source passed through a gold-coated glass tube (length 120 mm, and inside diameter 9.0 mm). The commercial CO_2 NDIR photodetector (Perkin-

Elmer TPS2734) had two thermopile elements, one of which was equipped with a band-pass filter at a wavelength of 4.3 μm for the measurement of the CO_2 absorption signal, whereas the other was equipped with a band-pass filter at a wavelength of 4.0 μm for the measurement of the background signal. The signals from the sensors were amplified by an operational amplifier and converted to 16 bit digital values by an A/D convertor. The signal intensities of the detectors at 4.0 and 4.3 μm without CO_2 gas were set to the equal levels by adjusting the amplification factors in the laboratory. The electric power for the CO_2 sensor, pump, and valves was supplied through a control board using three 9 V lithium batteries, lasted for more than 3 h during the flight. The control board connected to the components regulated the measurement procedures, such as switching the solenoid valves and processing the signal. As shown in Fig. **1**, the measurement system has an expanded polystyrene box molded specially to settle the optical absorption cell, electronic board, pump, battery and other components.

c. Calibration gas package

Under the wide ranges of temperature and pressure conditions, the CO_2 sensor signal was unstable, and the calibration of the CO_2 sensor only on the ground before launch was insufficient to obtain the precise values of the CO_2 concentrations. To solve this problem, an in-flight calibration system was incorporated into the CO_2 sonde. A calibration gas package was attached to the CO_2 sonde for the in-flight calibration, as shown in Fig. **2**. The calibration gas package consisted of two aluminum coated with polytetrafluoroethylene (PTFE) bags (maximum volume: 20 L), containing reference gases with low (~370 ppm) and high (~400 ppm) CO_2 concentrations. In each bag, ~8 L (STP) of the reference gas was introduced from standard CO_2 gas cylinders just before launch. Since the gas bags were soft, their inner pressures were equal with the ambient air pressures during the balloon flight. The gas volumes in the bags increased with the altitude during the ascent of the balloon due to a decrease in the ambient pressure, while the reference gases were consumed during the calibration procedures. The

optimum amounts of gas in the bags were determined by both the ascending speed of the balloon and the consumption rate to avoid the bursting of the bags and exhaustion of the gases. The CO_2 concentrations of the reference gases in the bags were checked by the NDIR instrument (LICOR, LI-840) before launching. Thereafter, approximately 6 L of the reference gas was left in each bag for a subsequent in-flight calibration. The change in the CO_2 mole fraction in the bags was less than 1 ppm over a 3 days period, which was negligible over the observations time during the balloon flight. All measurements were reported as dry-air mole fractions relative to the internally consistent standard scales maintained at Tohoku University (Tanaka et al. 1987; Nakazawa et al. 1992).

Since the gas exit port of the optical absorption cell was opened to the ambient air, the cell pressure was equalized with the ambient pressure for measuring both the ambient air and two standard gases. During the balloon-borne flights, the temperatures inside the CO_2 sonde package were measured with thermistors. The temperature inside the CO_2 sonde package gradually decreased by approximately 5 K, from 298 K on the ground to 293 K at an altitude of 10 km during the flights. Probably due to the polystyrene box, and the heat produced by the NDIR lamp, pump and solenoid valves, temperature inside the sonde package remained virtually constant in spite of low ambient temperatures at high altitudes (~220 K). Within one measurement cycle time (160 s) with the standard gases, the temperature change was less than 0.4 K in the sonde package. The temperatures of the sample gas in the tube just before the inlet of the CO_2 NDIR cell were also measured using a thin wire thermistor, commonly used for ambient temperature measurement in GPS sonde equipment with a quick response time (shorter than 2 s). The gas temperature change was negligible at the valve change timings between the standard gas and ambient air (< 0.1 K). The result indicated that the gas temperatures were relatively constant after passing through the valves, pump, dehumidifier cell, and piping for both the standard gases and ambient air.

The performances of the CO_2 sonde instruments were checked before the balloon launching since the CO_2 sonde systems were not recovered after the launch experiments were performed. For about 60

266 min. before the launch, the values of $[I(4.0) - I(4.3)]/P$ were measured with the valve cycles (each
267 step 40 s, total 160 s) for two standard gas packages (~370 ppm and ~400 ppm) for calibration and one
268 intermediate concentration gas package (~385 ppm) as a simulated ambient gas sample.
269
270 **d. Total sonde system**
271 The CO_2 sonde was equipped with a GPS radiosonde (Meisei Electric co., Ltd., RS-06G). The
272 balloon carried the instrument packages in the altitude with measuring CO_2 and meteorological data
273 (GPS position and time, temperature, pressure, and humidity). The CO_2 sonde transmitted those data
274 to a ground receiver (Meisei Electric co., Ltd., RD-08AC) at 1 s intervals, thus it was unnecessary to
275 recover the CO_2 sonde after the balloon burst. Figure **2** showed an overall view of the CO_2 sonde
276 developed in this study, which consisted of a CO_2 measurement package, a calibration gas package, a
277 GPS radiosonde, a balloon, and a parachute. The total weight of the CO_2 sonde was 1700 g, including
278 the GPS radiosonde (150 g), CO_2 measurement package (1000 g), and calibration gas package (550 g).
279 The dimensions of the CO_2 measurement package were width (W) 280 mm × height (H) 150 mm ×
280 depth (D) 280 mm. The size of the calibration gas package was W 400 mm × H 420 mm × D 490 mm.
281 The CO_2 sonde system was flown by a 1200 g rubber balloon (Totex). The ascending speed was
282 around 4 m / s by controlling the helium gas amount in the rubber balloon and checking the buoyancy
283 force. In practice, it was difficult to precisely control the ascending speed of the balloon, and the actual
284 resulting speeds were in the range of 3 - 5 m s^{-1}. This corresponds to the height resolution of
285 approximately 240–400 m for the measurements of the CO_2 vertical profiles.
286 Ascending speed slower than 3 m s^{-1} can lead to a collision with a nearby tree and building, result
287 in equipment falling in the urban areas. With faster ascending speeds, the altitude resolution of the
288 measurements decreased and the gas standard bag became full and the pressure inside the gas bags
289 became higher than the ambient pressure because of the lower ambient pressures at higher altitudes.
290 The high pressure inside the gas bag resulted in the fast flow speed in the optical absorption cell of

NDIR, which shifted the signal values for the pressurized gas sample. Since pressure relief valves for the bags did not work at low pressures at high altitudes, we did not use the pressure relief valve for the standard gas bags. When the ascending speed was low, the standard gas bags became empty since they were consumed by the in-flight calibration procedures during the long ascending time. Since the measurements after the over-pressurization or the exhaustion of the reference gas bag are useless, this technical problem determines the upper limit (10 km) of altitude for the measurements in this study. Based on our experiences, this problem generally occurred at an altitude above approximately 10 km. A prototype of the CO_2 sonde is available from Meisei Co. Ltd. (Isesaki, Japan) with about $4,500.

e. Data processing procedures

Since the surrounding conditions of the sonde change significantly during the ascending period, the NDIR measurement system is calibrated with the two standard gases at every altitudes. However, since the balloon-borne instrument is only equipped with one NDIR absorption cell and the balloon ascends continuously, it is not possible to measure the ambient air sample and the two standard gases at the same time and at the same altitude. Therefore, the measurement cycle during the flights consisted of the following steps: (1) low concentration standard gas, (2) ambient air, (3) high concentration standard gas, and (4) ambient air. The measurement time for each step was 40 s. At switching timings of the valve cycles, the signal became stable within 10 s, and the averages of residual 30-s period signals were used for the calculation of the CO_2 mole fractions. Since the gas exit port of the NDIR optical absorption cell was opened to the ambient air, the cell pressure was equalized with the ambient pressure. During the period of the 40 s gas change, the pressure would change about 2 % when the ascending speed of the balloon was 4 m s^{-1}. The temperature of the ambient air and standard gas samples at the inlet port of the optical cells was measured and found to be constant during each cycle of the calibration procedure.

Figure **3** shows an example of the raw data obtained from the CO_2 sonde experiment. Figure 3

316 presents the plots of the values of $[I(4.0)-I(4.3)]/P$ against the altitude, where $I(4.0)$ and $I(4.3)$
317 are the signal intensities at the wavelength of 4.0 μm for background measurements and the 4.3 μm
318 wavelength for CO_2 absorption measurements, as obtained by the NDIR CO_2 sensor on the balloon,
319 and P is the ambient atmospheric pressure obtained by the GPS sonde data and pressure
320 measurements on the ground.

321 The values of $[I(4.0)-I(4.3)]/P$ are proportional to the CO_2 mole fraction X according to the
322 Beer-Lambert law as expressed by Eq. (2). By using the values of $[I(4.0)-I(4.3)]/P$, we can
323 compensate for the pressure change to determine the CO_2 concentration. As shown in Fig. **3**, the
324 differences in the $[I(4.0)-I(4.3)]/P$ values between the low and high standard gases remained
325 relatively constant while ascending to the higher altitudes. However, the $[I(4.0)-I(4.3)]/P$ values
326 for the each standard gas did not change linearly but sometimes displayed some curvatures as shown
327 in Fig. **3**. This may be due to the differences between the baseline drift of the two sensors at 4.3 μm
328 and 4.0 μm in the NDIR detector. Since the measurements were performed alternately for the standard
329 gases and the ambient air with the NDIR cell and are not performed simultaneously, the values for the
330 standard gas signals at the time of the ambient air measurement was estimated. Therefore, the cubic
331 spline fitting curves for the observation points of the 30 s average values (red circles in Fig. **3**) of the
332 same standard gas were used to obtain the low and high calibration points for the calculation of the
333 mole fractions in the ambient air. In Fig. **3**, the cubic spline fitting curves are represented by the red
334 curves, and the estimated values for the standard gases at the ambient gas measuring time are
335 represented by the small black dots on the cubic spline curves, which are used for the interpolation to
336 determine the ambient air concentrations. Linear line fitting between the standard gas values did not
337 work well because the connection lines of the values sometimes displayed curvatures as shown in Fig.
338 **3**. Since there were in-phase fluctuations in the $I(4.0)$ and $I(4.3)$ signals during the flights, the
339 subtraction of $[I(4.0)-I(4.3)]$ could partly improve the signal-to-noise ratios by canceling in-phase
340 fluctuations with each other.

3. Results and discussion

a. Laboratory tests

Since the linear interpolation method for the $[I(4.0)-I(4.3)]/P$ values was used to determine the ambient air CO_2 mole fractions in the balloon-borne experiments, the deviations from the linear interpolation process were also investigated. The measurements of various mole fractions gas samples in the laboratory indicated that the linear interpolation error with the two standard gas packages (~370 ppm and ~400 ppm) was less than 0.2 ppm in the range between 360 and 410 ppm. Figure **4** shows the measurement results of the NDIR cell developed in this study at various CO_2 mole fractions. The outlet port of the NDIR system was connected to the commercial CO_2 instrument (LICOR, LI-840A) as a standard device, and the two instruments simultaneously measure the sample gas at 1010 hPa. The standard gases of 365 and 402 ppm were used for the calibration, and the mixtures of the standard gases were used for the samples. This indicated the values of $[I(4.0)-I(4.3)]/P$ of the system were proportional to the mole fraction of CO_2. This type of experiment could not be performed at low pressures, since we did not have a standard device which can be operated under low pressures.

Figure **5** shows the results of an experiment using a vacuum chamber in the laboratory, where the flight pressure conditions were simulated and the performances of the CO_2 sonde instruments was evaluated. The temperature inside the chamber was not controlled and was about 298 K. In the actual flights, the temperature inside the sonde package did not change more than 5 K. The CO_2 sonde system and two standard gas packages were placed in the vacuum chamber. The chamber was filled with the mole fraction sample gas of 377.3 ppm before the pumping. The pressure of the chamber was gradually and continuously decreased using a mechanical pump from 1010 hPa (ground surface pressure) to 250 hPa (about 10 km altitude pressure) over 60 min, corresponded to a balloon ascending speed of 3 m /s in actual flights, whereas the sample gas was slowly and continuously supplied to the chamber. The values $[I(4.0)-I(4.3)]/P$ were measured for the two standard gas packages, and the sample gas with

366 the valve cycles (each step 40 s, total 160 s) as described in the previous section. The mole fractions
367 of the sample gas in the chamber were calculated by the interpolation of the signals for the two standard
368 gases. The 30 s signals 10 s after the valve changes were used for the interpolation calculations to
369 avoid the incomplete gas exchanges in the NDIR optical cell. The black circle in Fig. **5** indicates the
370 sample gas mole fraction obtained from the linearly interpolated standard gas signals in each
371 calibration cycle. The vertical error bar in Fig. **5** indicates the square-root of the sum of squares for the
372 standard deviations of the sample and standard gas signals at each step. The errors in the CO_2 mole
373 fractions were estimated to be 0.6 ppm at 1010 hPa and 1.2 ppm at 250 hPa using the calibration cycles.
374 The results in Fig. 5 indicated that the determination of the sample gas concentration using the linear
375 interpolation with the standard gases was appropriate within the error, when the pressure continuously
376 decreased from 1000 to 250 ppm over 60 min.

377 When the CO_2 sonde instrument was inclined and vibrated in the laboratory, the fluctuations in the
378 signals were observed. The quantitative correlation between the signal fluctuation intensities and
379 acceleration speed, measured by a 3-dimensional acceleration sensor, was investigated, but no distinct
380 correlation was detected. However, the in-flight calibration system partly solved this problem by taking
381 the signal difference of $\left[I(4.0)-I(4.3)\right]$ and also by measuring alternately the two standard gases
382 every 40 s during the balloon flights.

383 The temperature characteristics of the CO_2 sensor were also investigated by changing the sensor cell
384 block temperature from 273 to 323 K at the pressure of ~1010 hPa, using a heater in the laboratory.
385 The laboratory experiment related to the temperature dependence suggested that the measurement error
386 is less than 0.2 ppm due to the temperature change during one valve cycle (160 s) in the balloon-borne
387 experiments.

388 In principle, the absorption intensities $\left(I_0 - I\right)$ in the NDIR measurements are proportional to the
389 absolute CO_2 concentrations in the sample air in the absorption cell. Therefore, at higher altitudes
390 where the pressures were lower, the values of $\left[I(4.0)-I(4.3)\right]$ were smaller and the signal-to-noise

391 ratios of $[I(4.0)-I(4.3)]/P$ decreased. The error of the CO_2 mole fractions of 1.2 ppm at 250 hPa
392 corresponds to an absolute CO_2 concentration of 3.2×10^{13} molecule cm^{-3}. The equivalent altitude for
393 this value was 90 km with a CO_2 molar fraction of 400 ppm. As described previously, the purpose of
394 CO_2 balloon observations is to measure the CO_2 mole fraction within 1 ppm errors in the atmospheres
395 around 400 ppm CO_2. The upper limit of the altitude for the observations with the developed CO_2
396 sonde is considered to be ~10 km. Furthermore, as described in section 2d, the problems of the vacancy
397 or over-pressure in the standard gas bags took place around 10 km altitudes, which resulted in large
398 errors. This also practically determines the upper altitude limit for CO_2 sonde observations.
399
400 **b. Comparison with aircraft data**
401 Two types of aircraft measurement data, the NIES/JAXA chartered aircraft and the CONTRAIL
402 data, were used for comparison with the CO_2 sonde measurement data. The NIES/JAXA chartered
403 aircraft measurements were conducted on the same days as the CO_2 sonde observations (January 31st,
404 2011 and February 3rd, 2011). The chartered aircraft observations were performed as a part of the
405 campaign for validating the GOSAT data and calibrating the TCCON FTS data at Tsukuba (36.05°N,
406 140.12°E) (Tanaka et al., 2012). The chartered aircraft data were obtained using an NDIR instrument
407 (LICOR LI-840) that had a control system of constant pressure and had the uncertainty of 0.2 ppm.
408 On both January 31st and February 3rd, the chartered aircraft measured the CO_2 mole fractions during
409 descent spirals over Tsukuba and Kumagaya (Fig. **6**). Because the air traffic was strictly regulated near
410 the Haneda and Narita international airports, the aircraft observations at altitudes above 2 km over
411 Tsukuba were prohibited. Therefore, the descent spiral observations were conducted over Kumagaya
412 at altitudes of 7–2 km and over Tsukuba at altitudes of 2–0.5 km. Tsukuba is located approximately 20
413 km northeast of Moriya, whereas Kumagaya is located approximately 70 km northwest of Moriya.
414 Seven profiles based on the CONTRAIL measurements, obtained during the ascent and descent of
415 aircrafts over Narita airport and had passage times close to the CO_2 sonde observations, were available

416 within two days after or before the dates of the CO_2 sonde measurements (Table 1). The CO_2 sonde
417 observations were conducted on January 31st and February 3rd, 2011 from Moriya. One set of
418 CONTRAIL data, obtained from the flight from Hong Kong to Narita (data set name: 11_060d), was
419 available on January 31st, but no CONTRAIL data were available for February 3rd. Therefore, the
420 CONTRAIL data, obtained from the flight from Hong Kong to Narita on February 2nd (data set name:
421 11_062d), were used for comparison with the February 3rd CO_2 sonde data. Figure **6** also shows the
422 CONTRAIL 11_060d and 11_062d flight paths and the CO_2 sonde launched at Moriya on January 31st
423 and February 3rd, 2011. On January 31st, the flight time of the CONTRAIL 11_060d over the Narita
424 airport and the launch time of the CO_2 sonde at Moriya were relatively close to one another. The flight
425 path of the CONTRAIL 11_062d data on February 2nd, 2011 was close to that of the CO_2 sonde on
426 February 3rd, 2011 and both observations were conducted in the early afternoon. The CONTRAIL
427 data referred in the present study was obtained using the Continuous CO_2 Measuring Equipment
428 (CME) located onboard commercial airliners (Machida et al. 2008; Matsueda et al. 2008). The typical
429 measurement uncertainty (1σ) of the CME has been reported as 0.2 ppm (Machida et al. 2008).
430 Figure **7** shows the vertical profiles of CO_2 observed by the CO_2 sonde at Moriya, the chartered
431 aircraft at Kumagaya and Tsukuba, and the CONTRAIL over the Narita airport on January 31st, 2011.
432 The overall vertical distribution of the CO_2 sonde data resembled with those of the chartered aircraft.
433 The vertical profiles of the CONTRAIL 11_060d flight on January 31st at the 5.3–6.8 km altitude
434 range consisted of the missing data because of the CME calibration period.
435 Figure **8** shows the comparison of the CO_2 vertical profiles obtained by the CO_2 sonde over Moriya,
436 NIES/JAXA chartered aircraft over Kumagaya and Tsukuba on February 3rd, 2011, and the
437 CONTRAIL on February 2nd, 2011 over Narita. The shape of the vertical profile obtained by the
438 chartered aircraft on February 3rd resembled that obtained by the CO_2 sonde, although the profile from
439 the chartered aircraft was shifted to the lower CO_2 concentration side compared to that of the CO_2
440 sonde.

441 Table 2 lists the comparisons of the CO_2 mole fractions measured by the balloon CO_2 sonde and
442 NIES/JAXA chartered aircraft on January 31st and February 3rd, 2011. The averaged values of the
443 aircraft measurement over the range of each balloon altitude ± 100 m are listed in Table 2, since the
444 altitude resolution of the aircraft measurements is higher than that of the CO_2 sonde. From the February
445 3rd measurements, the height of the boundary layer around an altitude of 1 km was different between
446 the CO_2 sonde and the NIES/JAXA aircraft measurements as shown in Fig. **8**. Therefore, the data
447 below 1 km on February 3rd are not included in Table 2. From the data on January 31st, the averaged
448 value of the differences between the CO_2 sonde and the NIES/JAXA aircraft was relatively small (0.42
449 ppm), which corresponded to the bias of the measurements. The standard deviation of the differences
450 was 1.24 ppm. From the February 3rd data, the bias was large (1.41 ppm), whereas the standard
451 deviation of the differences was not so large (1.00 ppm), which corresponded to the similar but shifted
452 vertical profiles in shapes between the CO_2 sonde and aircraft measurements as shown in Fig. **8**. The
453 difference between the CO_2 sonde data and the NIES/JAXA chartered aircraft data on February 3rd is
454 nearly equal to the difference between CONTRAIL data on February 2nd and the NIES/JAXA
455 chartered aircraft data on February 3rd.
456 Table 3 lists the comparisons of the CO_2 mole fractions measured by the balloon CO_2 sonde and
457 CONTRAIL aircraft, 11_060d on January 31st and 11_062d on February 2nd, 2011 up to the altitude
458 of 7,000 m. The averaged values of the aircraft measurements over the range of each balloon altitude
459 ± 100 m are listed in Table 3. The biases between the CO_2 sonde and the CONTRAIL aircraft results
460 were relatively small, 0.33 and 0.35 ppm, and the standard deviations of the differences were 1.16 and
461 1.30 ppm for the results on January 31st and February 3rd, respectively.
462 From the comparison between the CO_2 sonde data and the aircrafts (NIES/JAXA and CONTRAIL)
463 data, it was found that the CO_2 sonde observation was larger than those of aircrafts by about 0.6 ppm
464 on average. The standard deviation of the difference from the CO_2 sonde and aircraft observations was
465 1.2 ppm (1σ). If the 4 sets of aircraft measurement data obtained by the NIES/JAXA and CONTRAIL

observations were accurate within the published uncertainties, ignoring the differences in the flight time and geographical routes, the measurement error of the CO_2 sonde system was estimated from the standard deviations of all the difference values in Tables 2 and 3. The estimated error value up to an altitude of 7 km was 0.6 ± 1.2 ppm for the CO_2 sonde observation with a 240 m altitude resolution and 3 m s^{-1} ascending speed. The root mean square value (1.3 ppm) from all the difference value in Table 2 and 3 indicated that the CO_2 sonde could measure the CO_2 vertical profiles within 1.3 ppm on average compared to the aircraft observations. It is noted that, although error estimation was conducted for the data up to an altitude of 7 km due to the availability of the chartered aircraft data, the CO_2 sonde data above 7 km up to about 10 km. The measurement errors for the data above 7 km are expected to be larger than the above estimation.

c. CO_2 sonde observations over a forested area

Figure **9** shows the vertical profiles of the CO_2 mole fraction, temperature, and relative humidity obtained from the balloon-borne experiments of the CO_2 sonde at Moshiri (44.4°N, 142.3°E) on August 26, 2009. The launch site is in a rural area of Hokkaido, Japan and is surrounded by forests. The CO_2 sonde was launched at 13:29 LST and ascended with a mean vertical speed of approximately 3 m s^{-1}. The CO_2 sonde reached an altitude of 10 km after 56 min. The wind horizontally transported the CO_2 sonde distances of 10 km and 21 km northeast when the CO_2 sonde reached the altitudes of 5 km and 8 km, respectively. The CO_2 sonde rapidly moved 52 km southeast at an altitude of 16 km. Finally, the CO_2 sonde reached an altitude of 28 km before the balloon burst and the subsequent fall of the sonde was directed by the parachute into the Sea of Okhotsk located 80 km east of the launch site. The error bars for the CO_2 mole fraction in Fig. **9**a were calculated from the deviation of the signal intensities from the CO_2 sensor during the 40 s measurement periods for the ambient air and the two standard gases.

The vertical temperature profile in Fig. **9**b indicated the existence of three inversion layers of the

491 altitudes of approximately 2.0, 3.2, and 4.3 km. The relative humidity from the ground to the first
492 inversion layer at 2.0 km and between the second and third inversion layers from 3.2 to 4.3 km were
493 higher compared with those observed from 2.0 to 3.2 km and from 4.3 to 7.5 km. The CO_2 mole
494 fraction was the lowest near the ground (~373 ppm) and increased to approximately 384 ppm at an
495 altitude of 4–5 km around the third inversion layer before reaching a value of 387 ppm in the upper
496 troposphere (5–9 km). Significant decreases in the CO_2 mole fractions were observed in the two lower
497 layers from the ground to 3.2 km. Considering the clear weather on the day of the balloon experiment,
498 these results are explained by the uptake of CO_2 near the surface by plants in the forests through
499 photosynthesis processes in the daytime hours, and the diffusion and advection of the air mass
500 containing low CO_2 concentrations in the upper altitudes.
501 Because the CO_2 mole fraction for the vertical profiles near the surface is critically important to
502 estimating the flux around the observation point, the vertical profile data taken by our CO_2 sonde is
503 useful.
504
505 **d. CO_2 sonde observations over an urban area**
506 Figure **10** shows the vertical profiles of the CO_2 mole fraction, temperature, and relative humidity
507 obtained by the CO_2 sonde at Moriya (35.93°N, 140.00°E) on February 3rd, 2011. The launching time
508 was 13:10 LST and the sonde ascended with a mean vertical speed of approximately 2.9 m s^{-1}. Moriya
509 is located in the Kanto region and is 40 km northeast of the Tokyo metropolitan area. The launching
510 site was surrounded by the heavy traffic roads and residential areas. As seen in Fig. **10**a, high CO_2
511 mole fractions were observed from the ground up to an altitude of 1 km. The average CO_2 volume
512 mole fraction in this layer was higher than that measured in the free troposphere approximately above
513 15 ppm. A small temperature inversion layer appeared at approximately 1 km, and the maximum
514 relative humidity was observed just below this inversion layer (Figs. **10**b and c). These results
515 suggested that the CO_2 emitted from anthropogenic sources in and/or around the Tokyo metropolitan

area accumulated in the boundary layer at altitudes below 1 km.

An analysis of Figs. **9** and **10** indicated that there were a clear local consumption and emission of CO_2 from the comparison of the levels of CO_2 concentration in the free troposphere, which suggested a decoupling with the boundary-layer and synoptic inversion layers (Mayfield and Fochesatto, 2013). When a small increase in a column XCO_2 value is observed by a satellite, it is difficult to estimate which part of the atmosphere is responsible for the increase in XCO_2, the boundary layer with strong CO_2 emission in the nearby area, or the free troposphere. Considering this fact, the vertical profile data obtained by the CO_2 sonde around urban areas should provide more useful information than the column averaged observations obtained by the satellites and FTS measurements to estimate the flux of anthropogenic CO_2 emitted in and/or around the urban areas.

4. Conclusion

The CO_2 sonde is shown to be a feasible instrument for CO_2 measurements in the troposphere. The laboratory test with a vacuum chamber has shown the precision of the CO_2 sonde at ~1010 hPa for 0.6 ppm and at ~250 hPa for 1.2 ppm. Comparisons of the CO_2 vertical profiles obtained by the CO_2 sonde with two types of aircraft observations, the CONTRAIL and the NIES/JAXA chartered aircraft, were carried out. The CO_2 sonde and CONTRAIL data were consistent. The CO_2 sonde data on January 31st, 2011 was in good agreement with the chartered aircraft data on the same day, but the CO_2 sonde data observed on February 3rd, 2011 was larger by approximately 1.4 ppm, as compared with the chartered aircraft data obtained on the same day from the ground to an altitude of 7 km. The measurement errors of the CO_2 sonde system up to an altitude of 7 km were estimated to be 1.4 ppm for a single point of 80 s period measurements with a vertical height resolution of 240–400 m. We conducted the field CO_2 sonde observations more than 20 times in Japan and successfully obtained CO_2 vertical profiles from the ground up to altitudes of approximately 10 km.

Our results showed that low-cost CO_2 sondes could potentially be used for frequent measurements

of vertical profiles of CO_2 in many parts of the world providing as useful information to understand the global and regional carbon budgets by replenishing the present sparse observation coverage. The CO_2 sondes can detect the local and regional transport evidence by determining CO_2 concentrations in the air layer trapped between elevated inversion layers. Also, the CO_2 sonde observation data could help improve the inter-comparison exercise for inverse models and for the partial validation of satellite column integral data. In future, the CO_2 sonde data will be used for the validation of satellites and the calibration of ground-based observations of sunlight spectroscopic measurements for column values of CO_2 concentration.

Acknowledgments

We would like to thank N. Toriyama, M. Kanada, H. Jindo, M. Sera, H. Sasago, T. Ide, S. Takekawa, M. Kawasaki, G. Inoue (Nagoya Univ.), M. Fujiwara, Y. Inai (Hokkaido Univ.), S. Aoki, and T. Nakazawa (Tohoku Univ.) for their assistance and useful suggestions in the development of CO_2 sonde and the observations. This work was partly supported by the Grant-in-Aid for Scientific Research (KAKENHI 20310008 and 24310012), Green Network of Excellence, Environmental Information (GRENE-ei) program from the Ministry of Education, Culture, Sports, Science and Technology (MEXT), Development of Systems and Technology for Advanced Measurement and Analysis Program from Japan Science and Technology Agency (JST), and the joint research program of the Solar-Terrestrial Environment Laboratory (Now new organization: the Institute for Space-Earth Environmental Research), Nagoya University.

562 **References**

563 Ahmadov, R., Gerbig, C., Kretschmer, R., Körner, S., Rödenbeck, C., Bousquet, P., and Ramonet,
564 M.: Comparing high resolution WRF-VPRM simulation and two global CO_2 transport models
565 with coastal tower measurements of CO_2, Biogeosciences, **6**, 807–817, doi:10.5194/bg-6-807-
566 2009, 2009.

567 Andrews, A. E. and Coauthors: CO_2, CO, and CH_4 measurements from tall towers in the NOAA
568 Earth System Research Laboratorys Global Greenh ouse Gas Reference Network:
569 instrumentation, uncertainty analysis, and recommendations for future high-accuracy greenhouse
570 gas monitoring efforts, Atmos. Meas. Tech., **7**, 647-687, doi:10.5194/amt-7-647-2014, 2014.

571 Baker, D. F. and Coauthors: TransCom 3 inversion intercomparison: Impact of transport model errors
572 on the interannual variability of regional CO_2 fluxes, 1988–2003, Global Biogeochem. Cycles, **20**,
573 GB1002, doi:10.1029/2004GB002439, 2006.

574 Bakwin, P. S., Tans, P. P., Zhao, C., Ussler III, W., and Quesnell, E.: Measurements of carbon dioxide
575 on a very tall tower, Tellus **47B**, 535-549, 1995, doi:10.1034/j.1600-0889.47.issue5.2.x, 2002.

576 Chédin, A., Serrar, S., Armante, R., Scott, N. A., and Hollingsworth, A.: Signatures of annual and
577 seasonal variations of CO_2 and other greenhouse gases from comparisons between NOAA TOVS
578 observations and radiation model simulations, J. Climate, **15**, 95-116, doi:10.1175/1520-
579 0442(2002)015<0095:SOAASV>2.0.CO;2, 2002.

580 Conway, T. J., Tans, P. P., Waterman, L. S., Thoning, K. W., Masarie, K. A., and Gammon, R. H.:
581 Atmospheric carbon dioxide measurements in the remote global troposphere, 1981–1984, *Tellus*
582 *B*, **40**, 81–115, doi:10.1111/j.1600-0889.1988.tb00214.x., 1988.

583 Conway, T. J., Tans, P. P., Waterman, L. S., Thoning, K. W., Kitzis, D. R., Masarie, K. A. and Zhang,
584 N.: Evidence for interannual variability of the carbon cycle from the National Oceanic and
585 Atmospheric Administration/Climate Monitoring and Diagnostics Laboratory global air sampling
586 network, J. Geophys. Res., **99**(D11), 22,831–22,855, doi:10.1029/94JD01951, 1994.

587 Crevoisier, C., Heilliette, S., Chédin, A., Serrar, S., Armante, R. and Scott, N. A.: Midtropospheric
588 CO_2 concentration retrieval from AIRS observations in the tropics, Geophys. Res. Let., **31**,
589 L17106, doi:10.1029/2004GL020141, 2004.
590 Daube, B. C., Boering, K. A., Andrews, A. E. and Wofsy, S. C.: A high-precision fast-response
591 airborne CO_2 analyzer for in situ sampling from the surface to the middle stratosphere, J.
592 Atmospheric Ocean. Technol., **19**(10), 1532-1543, doi:10.1175/1520-0426(2002)019
593 <1532:AHPFRA>2.0.CO;2, 2002.
594 Dils, B. and Coauthors: Comparisons between SCIAMACHY and ground-based FTIR data for total
595 columns of CO, CH_4, CO_2 and N_2O, Atmos. Chem. Phys., **6**, 1953–1976, doi:10.5194/acp-6-1953-
596 2006, 2006.
597 Durry, G., Amarouche, N., Zéninari, V., Parvitte, B., Lebarbu, T. and Ovarlez, J.: In situ sensing of
598 the middle atmosphere with balloon borne near-infrared laser diodes, Spectrochimica Acta Part A,
599 **60**, 3371–3379, doi:10.1016/j.saa.2003.11.050, 2004.
600 Eldering, A. and Coauthors: The Orbiting Carbon Observatory-2: first 18 months of science data
601 products, Atmos. Meas. Tech., **10**, 549-563, doi:10.5194/amt-10-549-2017, 2017.
602 Fang, S. X., Zhou, L. X., Tans, P. P., Ciais, P., Steinbacher, M., Xu, L., and Luan, T.: In situ
603 measurement of atmospheric CO_2 at the four WMO/GAW stations in China, Atmos. Chem. Phys.,
604 14, 2541–2554, doi:10.5194/acp-14-2541-2014, 2014.
605 Galais, A., Fortunato, G. and Chavel, P: Gas concentration measurement by spectral correlation:
606 rejection of interferent species, Appl. Opt., **24**, 2127-2134, doi:10.1364/ao.24.002127, 1985.
607 Gurney, K. R. and Coauthors: Towards robust regional estimates of CO_2 sources and sinks using
608 atmospheric transport models, Nature, **415**, 626-630, doi:10.1038/415626a, 2002.
609 Gurney, K. R. and Coauthors: Transcom 3 inversion intercomparison: Model mean results for the
610 estimation of seasonal carbon sources and sinks. Global Biogeochem. Cycles, **18**, GB1010,
611 doi:10.1029/2003GB002111, 2004.

612 Ghysels, M., Durry, G., Amarouche, N., Cousin, J., Joly, L., Riviere, E. D., and Beaumont, L.: A
613 lightweight balloon-borne laser diode sensor for the in situ measurement of CO_2 at 2.68 micron in
614 the upper troposphere and the lower stratosphere, Appl. Phys. B, **107**, 213-220,
615 doi:10.1007/s00340-012-4887-y, 2012.
616 Hodgkinson, J., Smith, R., Ho, Wah On, Saffell, J. R.. Tatam, R. P.: Non-dispersive infra-red (NDIR)
617 measurement of carbon dioxide at 4.2 μm in a compact and optically efficient sensor, Sensors and
618 Actuators B, **186**, 580– 588. doi: 10.1016/j.snb.2013.06.006, 2013.
619 Inai Y., Aoki, S., Honda, H., Furutani, H., Matsumi, Y., Ouchi, M., Sugawara, S., Hasebe, F.,
620 Uematsu, M., Fujiwara, M.: Balloon-borne tropospheric CO_2 observations over the equatorial
621 eastern and western Pacific, Atmos. Env., **184**, 24-36. doi: 10.1016/j.atmosenv.2018.04.016, 2018.
622 Inoue, H. Y., and Matsueda, H.: Measurements of atmospheric CO_2 from a meteorological tower in
623 Tsukuba, Japan. Tellus, **53B**, 205–219, doi:10.1034/j.1600-0889.2001.01163.x, 2001.
624 Joly. L., Parvitte, B., Zeninari, V. and Durry, G.: Development of a compact CO_2 sensor open to the
625 atmosphere and based on near-infrared laser technology at 2.68 μm, Appl. Phys. B, **86**, 743–748,
626 doi:10.1007/s00340-006-2568-4, 2007.
627 Karion, A., C. Sweeney, P. Tans, and T. Newberger, 2010: AirCore: An innovative atmospheric
628 sampling system, *J. Atmos. Oceanic Technol.,* **27**, 1839–1853, doi:10.1175/2010JTECHA1448.1.
629 Komhyr, W. D., Harris, T. B., Waterman, L. S., Chin, J. F. S. and Thoning, K. W.: Atmospheric
630 carbon dioxide at Mauna Loa Observatory 1. NOAA global monitoring for climatic change
631 measurements with a nondispersive infrared analyzer, 1974–1985, J. Geophys. Res., **94**, 8533–
632 8547, doi:10.1029/JD094iD06p08533, 1989.
633 Machida, T., Matsueda, H., Sawa, Y., Nakagawa, Y., Hirotani, K., Kondo, N., Goto, K., Ishikawa, K.,
634 Nakazawa, T., and Ogawa, T.: Worldwide measurements of atmospheric CO_2 and other trace gas
635 species using commercial airlines, J. Atmos. Oceanic Technol., **25**(10), 1744–1754,
636 doi:10.1175/2008JTECHA1082.1, 2008.

637 Maksyutov, S., Nikolay, K., Nakatsuka, Y., Patra, P. K., Nakazawa, T., Yokota, T., and Inoue, G.:
638 Projected Impact of the GOSAT observations on regional CO_2 flux estimations as a function of
639 total retrieval error. J. Remote Sensing Soc. Japan, **28**, 190-197, doi:10.11440/rssj.28.190, 2008.
640 Matsueda, H., Machida, T., Sawa, Y., Nakagawa, Y., Hirotani, K., Ikeda, H., Kondo, N., and Goto,
641 K.: Evaluation of atmospheric CO_2 measurements from new flask air sampling of JAL airliner
642 observations. Pap. Meteor. Geophys., **59**, 1–17, doi:10.2467/mripapers.59.1, 2008.
643 Mayfield J. A. and Fochesatto, G. J.: The Layered Structure of the winter Atmospheric Boundary Layer in the
644 Interior of Alaska. J. Appl. Met. Climatol., 52, 953-973, doi.org/10.1007/s00703-013-0274-4, 2013.
645 Morino, I. and Coauthors, 2011: Preliminary validation of column-averaged volume mixing ratios of
646 carbon dioxide and methane retrieved from GOSAT short-wavelength infrared spectra, Atmos.
647 Meas. Tech., **4**, 1061–1076, doi:10.5194/amt-4-1061-2011.
648 Nakazawa, T., Murayama, S., Miyashita, K., Aoki, S., and Tanaka, M.: Longitudinally different
649 variations of lower tropospheric carbon dioxide concentrations over the North Pacific Ocean,
650 Tellus, **44B**, 161–172, doi:10.3402/tellusb.v44i3.15438, 1992
651 Nakazawa, T., Machida, T., Sugawara, S., Murayama, S., Morimoto, S., Hashida, G., Honda, H. and
652 Itoh, T.: Measurements of the stratospheric carbon dioxide concentration over Japan using a
653 balloon-borne cryogenic sampler, Geophys. Res. Letter, **22**, 1229–1232, doi:10.1029/95GL0118,
654 1995.
655 Pales, J. C., and Keeling, C. D.: The concentration of atmospheric carbon dioxide in Hawaii, J.
656 Geophys. Res., **70**, 6053-6076, doi:10.1029/JZ070i024p06053, 1965.
657 Stephens, B. B. and Coauthors: Weak northern and strong tropical land carbon uptake from vertical
658 profiles of atmospheric CO_2, Science, **316**, 1732–1735, doi:10.1126/science.1137004, 2007.
659 Sweeney, C. and Coauthors: Seasonal climatology of CO_2 across North America from aircraft
660 measurements in the NOAA/ESRL Global Greenhouse Gas Reference Network, J. Geophys. Res.,
661 **120**, 5155-5190, doi:10.1002/2014JD022591, 2014.

662 Tanaka, M., Nakazawa, T. and Aoki, S.: High quality measurements of the concentration of
663 atmospheric carbon dioxide. *J. Meteor. Soc. Japan*, **61**, 678-685, doi:10.2151/jmsj1965.61.4_678,
664 1983.
665 Tanaka, M., Nakazawa, T. and Aoki S.: Time and space variations of tropospheric carbon dioxide
666 over Japan, Tellus, **39B**, 3–12, doi:10.3402/tellusb.v39i1-2.15318, 1987.
667 Tanaka, T., Miyamoto, Y., Morino, I., Machida, T., Nagahama, T., Sawa, Y., Matsueda, H., Wunch,
668 D., Kawakami, S., and Uchino, O.: Aircraft measurements of carbon dioxide and methane for the
669 calibration of ground-based high-resolution Fourier Transform Spectrometers and a comparison to
670 GOSAT data measured over Tsukuba and Moshiri. Atmos. Meas. Tech., **5**, 2003–2012,
671 doi:10.5194/amt-5-2003-2012, 2012.
672 Tans, P. P., Conway, T., and Nakazawa T.: Latitudinal distribution of the sources and sinks of
673 atmospheric carbon dioxide derived from surface observations and an Atmospheric Transport
674 Model, J. Geophys. Res., **94**, 5151–5172, doi:10.1029/JD094iD04p05151, 1989.
675 Watai, T., Machida, T., Ishizaki, N. and Inoue, G.: A lightweight observation system for atmospheric
676 carbon dioxide concentration using a small unmanned aerial vehicle, J. Atmos. Oceanic Technol.,
677 **23**, 700–710 doi:10.1175/JTECH1866.1, 2006.
678 Winderlich, J., Chen, H., Gerbig, C., Seifert, T., Kolle, O., Lavrič, J. V., Kaiser, C., Höfer, A., and
679 Heimann, M.: Continuous low-maintenance CO_2/CH_4/H_2O measurements at the Zotino Tall
680 Tower Observatory (ZOTTO) in Central Siberia, Atmos. Meas. Tech., **3**, 1113–1128,
681 doi:10.5194/amt-3-1113-2010, 2010.
682 WMO: The state of greenhouse gases in the atmosphere using global observations through 2015,
683 WMO Greenhouse Gas Bull., **12**, 1–8, 2016.
684 Wofsy, S. C., the HIPPO science team and cooperating modellers and satellite teams: HIAPER Pole-
685 to-Pole Observations (HIPPO): fine-grained, global-scale measurements of climatically important
686 atmospheric gases and aerosols, Phil. Trans. R. Soc. A, **369**, 2073–2086,

687 doi:10.1098/rsta.2010.0313, 2011.
688 Wunch, D., Toon, G. C., Blavier, J. L., Washenfelder, R. A., Notholt, J., Connor, B. J., Griffith, D. W.
689 T., Sherlock, V. and Wennberg, P. O.: The Total Carbon Column Observing Network. Phil. Trans.
690 R. Soc. A, **369**, 2087–2112, doi:10.1098/rsta.2010.0240, 2011.
691 Yokota, T., Yoshida, Y., Eguchi, N., Ota, Y., Tanaka, T., Watanabe, H. and Maksyutov, S.: Global
692 concentrations of CO_2 and CH_4 retrieved from GOSAT: First preliminary results, Sci. Online Lett.
693 Atmos., **5**, 160–163, doi:10.2151/sola.2009–041, 2009.
694 Yoshida, Y., Ota, Y., Eguchi, N., Kikuchi, N., Nobuta, K., Tran, H., Morino, I., and Yokota, T.:
695 Retrieval algorithm for CO_2 and CH_4 column abundances from short-wavelength infrared spectral
696 observations by the Greenhouse gases observing satellite, Atmos. Meas. Tech., **4**, 717–734,
697 doi:10.5194/amt-4-717-2011, 2011.
698

699 **Table 1**. CONTAIL flight data near to the CO_2 sonde measurements on 31 January and 3 February

700 2011.

701

702

Data set name	Date	Time (LST)[a]
11_057a	CONTRAIL (29 January)	19:01
11_058d	CONTRAIL (30 January)	15:06
11_059a	CONTRAIL (30 January)	18:46
11_060d	CONTRAIL (31 January)	15:07
11_061a	CONTRAIL (1 February)	18:46
11_062d	CONTRAIL (2 February)	14:58
11_063a	CONTRAIL (4 February)	18:58
	CO_2 sonde (31 January)	13:06
	CO_2 sonde (3 February)	13:10

703

704 [a] Time for the CONTRAIL data represents the flight time in Japan Standard Time at an altitude of 1

705 km over the Narita airport. Time for the CO_2 sonde data represents the launching time at Moriya.

706

707

708

Table 2. Comparisons of the CO_2 mole fractions between the balloon CO_2 sonde and NIES/JAXA chartered aircraft measurements on 31st January and 3rd February 2011.

JAXA-NIES Chartered Aircraft (31 January 2011)				JAXA-NIES Chartered Aircraft (3 February 2011)			
Altitude (m)[a]	Balloon CO_2 (ppm)	Aircraft CO_2 (ppm)[b]	Difference (ppm)[c]	Altitude (m)[a]	Balloon CO_2 (ppm)	Aircraft CO_2 (ppm)[b]	Difference (ppm)[c]
849	399.05	397.62	1.43	1324	396.60	394.45	2.15
1202	398.16	397.53	0.63	1612	394.65	393.03	1.62
1610	398.00	397.17	0.83	1917	394.86	394.10	0.76
2038	396.50	396.95	-0.45	2223	395.77	393.54	2.23
2291	398.03	396.04	1.99	2539	395.41	393.95	1.45
2463	396.54	395.65	0.89	2867	394.71	395.11	-0.40
2844	393.44	395.24	-1.79	3215	394.99	392.99	2.00
3329	395.45	394.15	1.30	3543	393.59	393.07	0.52
3732	393.51	393.63	-0.12	3764	393.69	393.40	0.28
4161	395.47	393.54	1.93	3938	395.15	393.11	2.04
4575	394.62	392.94	1.68	4169	393.83	392.68	1.15
4918	393.24	393.64	-0.41	4458	396.57	393.51	3.06
5273	392.41	393.25	-0.84	4750	394.88	393.69	1.19
5654	393.02	393.47	-0.45	5047	396.53	394.01	2.53
6083	391.87	392.91	-1.04	5214	395.91	393.45	2.46
6510	392.76	391.65	1.11	5383	396.78	393.58	3.20
		Average =	0.42	5565	395.83	393.67	2.15
		Std Dev[d] =	1.16	5781	395.18	393.39	1.80
		RMS[e] =	1.20	6092	391.75	392.83	-1.09
				6287	392.44	392.42	0.02
				6467	393.67	392.23	1.44
				6639	395.07	392.42	2.65
				6815	394.00	393.00	1.00
						Average =	1.41
						Std Dev[d] =	1.00
						RMS[e] =	1.62

a. Altitudes of the balloon-borne experiments using the in-flight calibration with 40-s time intervals.

b. Averaged values of the aircraft measurement results over the range of the balloon altitudes ± 100 m.

c. Difference values of [balloon CO_2] - [Aircraft CO_2]

d. Standard deviation of the differences (1σ).

e. Root mean square values.

718 **Table 3.** Comparisons of the CO_2 mole fractions between the balloon CO_2 sonde measurements on
719 31 January and CONTRAIL aircraft CME on 31 January (11_060d) and between the CO_2 sonde on 3
720 February and CONTRAIL on 2 February (11_062d) up to the altitude of 7 km. The annotations are
721 same as Table 2.
722

CONTRAIL 11_060d (31 January 2011)				CONTRAIL 11_062d (2 February 2011)			
Altitude (m)	Balloon CO_2 (ppm)	Aircraft CO_2 (ppm)	Difference (ppm)	Altitude (m)	Balloon CO_2 (ppm)	Aircraft CO_2 (ppm)	Difference (ppm)
849	399.05	398.21	0.84	1917	394.86	396.59	-1.73
1202	398.16	399.56	-1.40	2223	395.77	396.45	-0.68
1610	398.00	398.77	-0.76	2539	395.41	395.71	-0.30
2038	396.50	397.07	-0.57	2867	394.71	394.67	0.04
2291	398.03	395.97	2.06	3215	394.99	393.34	1.65
2463	396.54	394.55	1.99	3543	393.59	394.25	-0.66
2844	393.44	393.41	0.04	3764	393.69	394.33	-0.64
3329	395.45	394.25	1.20	3938	395.15	394.69	0.46
3732	393.51	393.58	-0.07	4458	396.57	394.09	2.48
4161	395.47	393.86	1.61	4750	394.88	395.02	-0.14
4575	394.62	393.18	1.44	5047	396.53	396.55	-0.01
4918	393.24	393.62	-0.38	5214	395.91	396.01	-0.10
5273	392.41	392.76	-0.35	5383	396.78	394.78	2.00
6866	392.31	393.26	-0.96	5565	395.83	393.69	2.14
		Average =	0.33	5781	395.18	393.79	1.39
		Std Dev =	1.16	6092	391.75	393.57	-1.82
		RMS =	1.17	6287	392.44	393.32	-0.88
				6467	393.67	392.89	0.78
				6639	395.07	392.84	2.23
				6815	394.00	393.11	0.90
						Average =	0.35
						Std Dev =	1.30
						RMS =	1.31

723
724

725 **Figure captions**

726 **Figure 1.** Left: Schematic diagram of the CO_2 measurement package, where F1 and F2 represent the
727 band-pass filters at wavelengths of 4.0 μm and 4.3 μm, respectively. The outlet port of the CO_2 sensor
728 is opened to ambient air. Details of the system are described in the text. Right: Photograph of the inside
729 of the CO_2 sonde package. The components were placed in a specially modeled expanded polystyrene
730 box.

731 **Figure 2**. Photograph of the CO_2 sonde developed in this study before launching. a. CO_2
732 measurement package is shown in Fig. **1**, b. GPS sonde, and c. Calibration gas package.

733 **Figure 3**. Raw data obtained by the CO_2 sonde launched on September 26, 2011 at Moriya, Japan. The
734 vertical axis is the difference between the 4.0 μm and 4.3 μm signal intensities divided by the ambient
735 pressure. The black line indicates the observation results during the balloon flight with calibration
736 cycles. The red circle indicates the 30 s average values in each step of the calibration. Red curve
737 indicates the cubic spline fitting curves for the observation points of the 30 s average values of the
738 same standard gas. The small black dots on the cubic spline curves indicate the estimated values for
739 the standard gases at the ambient gas measuring timing, which were is used for the interpolation to
740 determine the ambient air concentrations.

741 **Figure 4.** $[I(4.0) - I(4.3)]/P$ values versus CO_2 mole fraction, where $I(4.0)$ and $I(4.3)$ are the
742 signal intensities at the 4.0 μm wavelength for background measurements and the 4.3 μm wavelength
743 for CO_2 absorption measurements, obtained by the NDIR CO_2 sensor, and P is the ambient
744 atmospheric pressure. CO_2 mole fractions were measured with a standard NDIR instrument (LICOR,
745 LI-840A) connected to the balloon sensor in series. The pressure while carrying out the
746 measurements was constant at 1010 hPa.

747 **Figure 5**. Results of a chamber experiment of the CO_2 sonde. Pressure in the chamber was reduced
748 from 1010 hPa (ground level pressure) to 250 hPa (about 10 km altitude pressure) at a temperature of
749 about 298 K. The black circles indicate the value of the CO_2 mole fraction of the sample air in the

chamber, which was obtained from the interpolation of the standard gas values in each calibration cycle. Vertical error bars indicate the square-root of sum of squares for the standard deviations of the sample and standard gas signals at each step in the calibration cycle. The black dashed line shows an average of all the values obtained for the sample gas. See the text for more details.

Figure 6. Flight paths of the CO_2 sonde observations launched at Moriya on January 31st (blue solid line) and February 3rd (red solid line), 2011, the CONTRAIL 11_060d data on January 31st, 2011 (black solid line) and 11_062d data on February 2nd, 2011 (black dashed line) from Hong Kong to Narita, and the NIES/JAXA chartered aircraft experiment on January 31st (green solid line) and February 3rd (purple dotted line). The altitudes of the flight paths are also indicated.

Figure 7. The CO_2 vertical profiles obtained by the CO_2 sonde (circles connected with blue lines), NIES/JAXA chartered aircraft data (dots connected with green lines), and the CONTRAIL data (diamonds connected with black lines) on January 31st, 2011.

Figure 8. The CO_2 vertical profiles obtained by the CO_2 sonde (circles connected with red lines), NIES/JAXA chartered aircraft data (dots connected with purple lines) on February 3rd, and CONTRAIL data (diamonds connected with black lines) on February 2nd, 2011.

Figure 9. Profiles of (a) CO_2 mole fraction, (b) temperature (solid line) and potential temperature (dotted line), and (c) relative humidity observed over a forest area, Moshiri in Hokkaido, Japan by the balloon launched on August 26, 2009 at 13:30 (LST). The black circles with error bars in panel (a) represent the data obtained by the CO_2 sonde.

Figure 10. Profiles of (a) CO_2 mole fraction, (b) temperature (solid line) and potential temperature (dotted line), and (c) relative humidity observed over an urban area, Moriya near Tokyo on February 3rd, 2011 at 13:10 (LST).

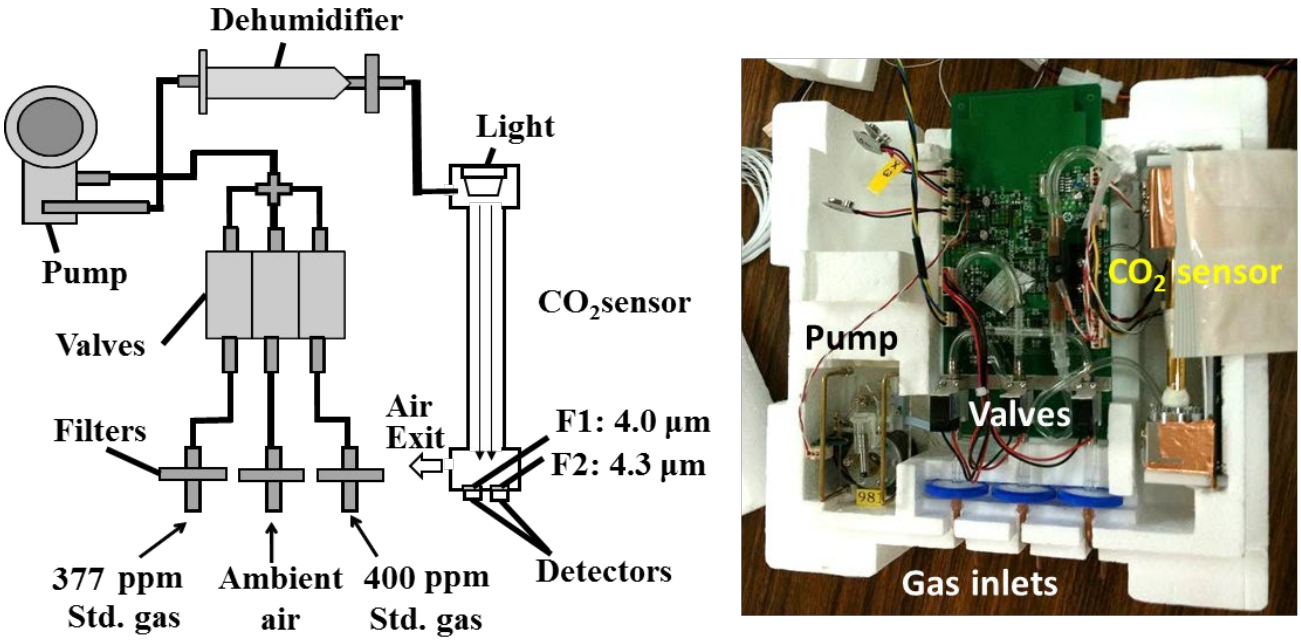

Figure 1. Left: Schematic diagram of the CO_2 measurement package, where F1 and F2 represent the band-pass filters at wavelengths of 4.0 µm and 4.3 µm, respectively. The outlet port of the CO_2 sensor is opened to ambient air. Details of the system are described in the text. Right: Photograph of the inside of the CO_2 sonde package. The components were placed in a specially modeled expanded polystyrene box.

782

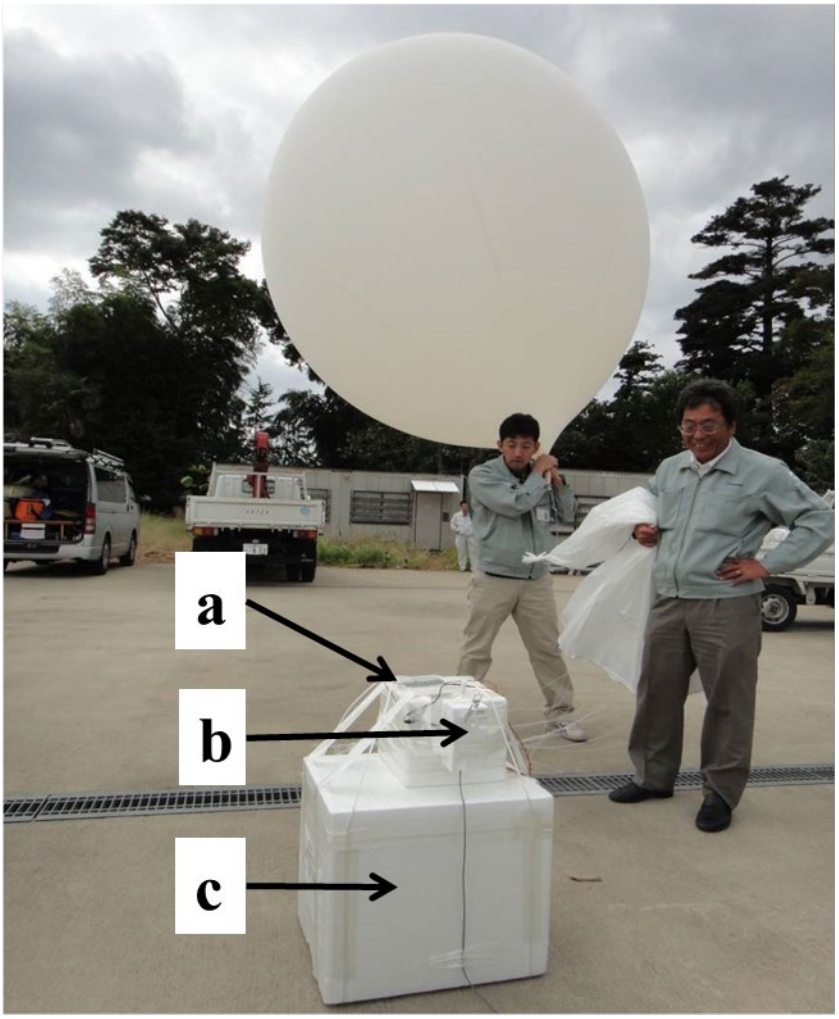

783

784 **Figure 2**. Photograph of the CO_2 sonde developed in this study before launching. a. CO_2

785 measurement package is shown in Fig. **1**, b. GPS sonde, and c. Calibration gas package.

786

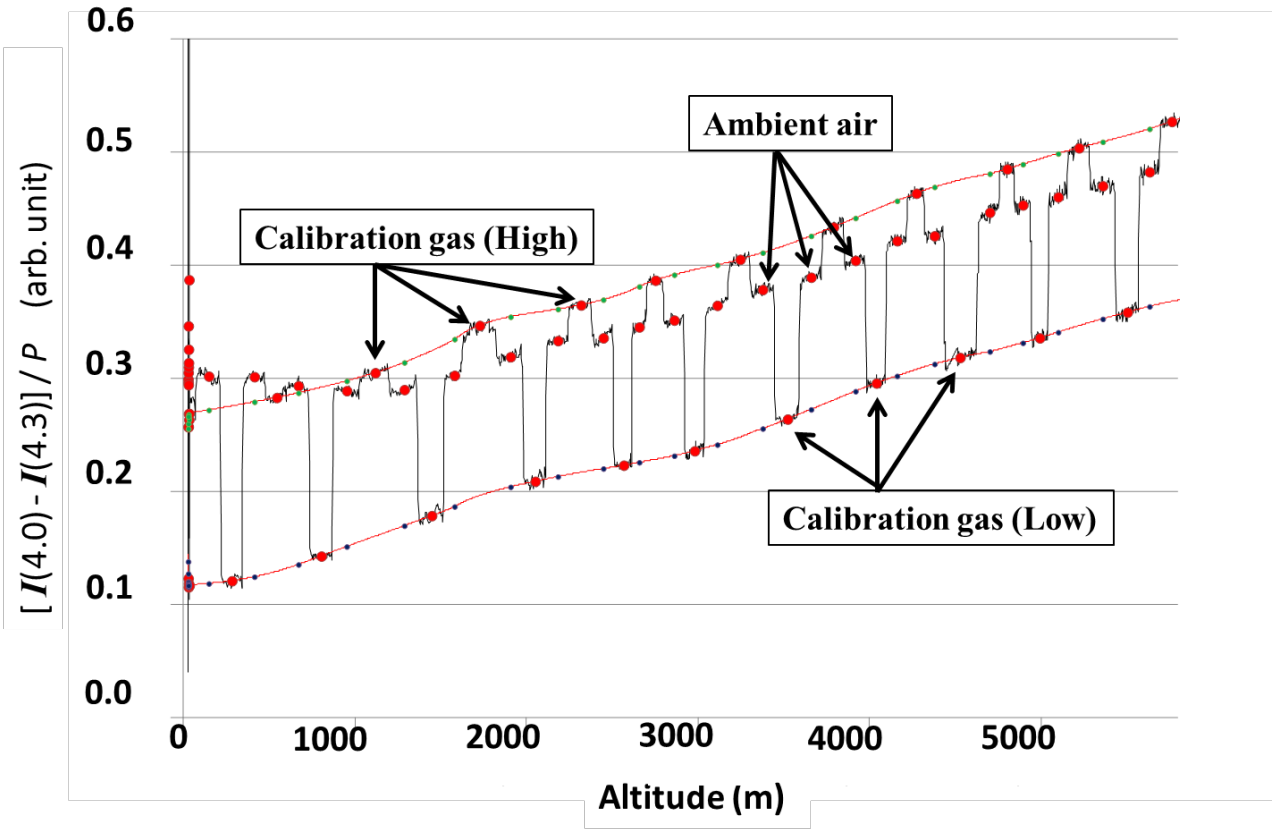

787 **Figure 3**. Raw data obtained by the CO_2 sonde launched on September 26, 2011 at Moriya, Japan.
788 The vertical axis is the difference between the 4.0 μm and 4.3 μm signal intensities divided by the
789 ambient pressure. The black line indicates the observation results during the balloon flight with
790 calibration cycles. The red circle indicates the 30 s average values in each step of the calibration. Red
791 curve indicates the cubic spline fitting curves for the observation points of the 30 s average values of
792 the same standard gas. The small black dots on the cubic spline curves indicate the estimated values
793 for the standard gases at the ambient gas measuring timing, which were is used for the interpolation
794 to determine the ambient air concentrations.
795
796

797

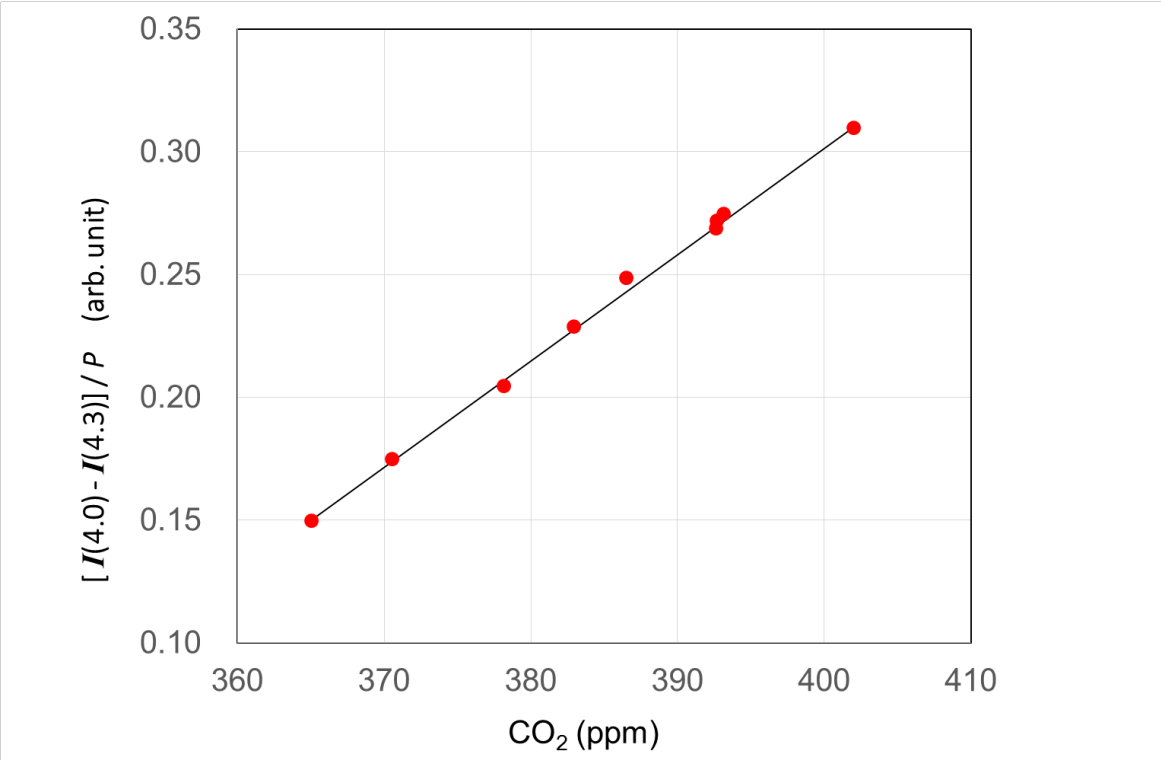

798

799 **Figure 4.** $[I(4.0)-I(4.3)]/P$ values versus CO_2 mole fraction, where $I(4.0)$ and $I(4.3)$ are the

800 signal intensities at the 4.0 μm wavelength for background measurements and the 4.3 μm wavelength

801 for CO_2 absorption measurements, obtained by the NDIR CO_2 sensor, and P is the ambient

802 atmospheric pressure. CO_2 mole fractions were measured with a standard NDIR instrument (LICOR,

803 LI-840A) connected to the balloon sensor in series. The pressure while carrying out the

804 measurements was constant at 1010 hPa.

805

806

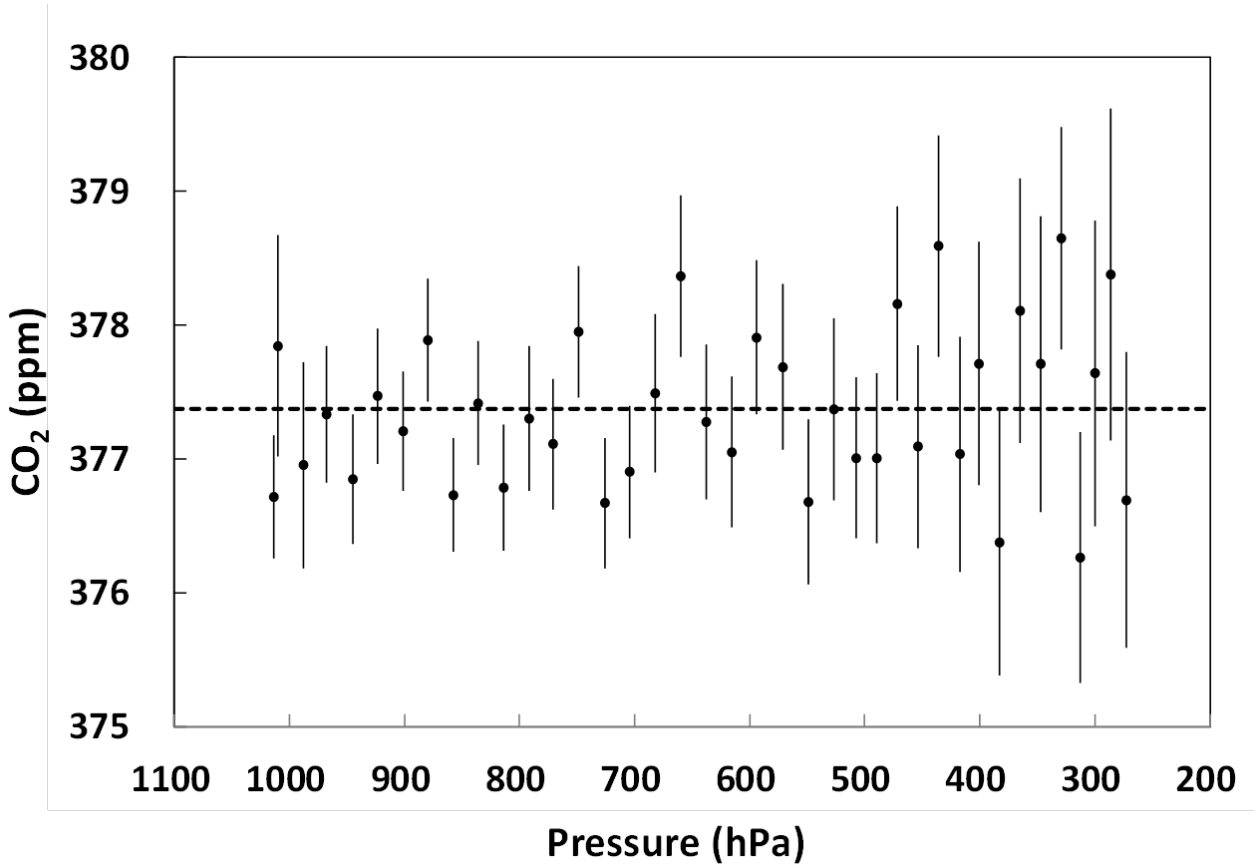

807

808

809 **Figure 5**. Results of a chamber experiment of the CO_2 sonde. Pressure in the chamber was reduced
810 from 1010 hPa (ground level pressure) to 250 hPa (about 10 km altitude pressure) at a temperature of
811 about 298 K. The black circles indicate the value of the CO_2 mole fraction of the sample air in the
812 chamber, which was obtained from the interpolation of the standard gas values in each calibration
813 cycle. Vertical error bars indicate the square-root of sum of squares for the standard deviations of
814 the sample and standard gas signals at each step in the calibration cycle. The black dashed line shows
815 an average of all the values obtained for the sample gas. See the text for more details.

816

817

818

819

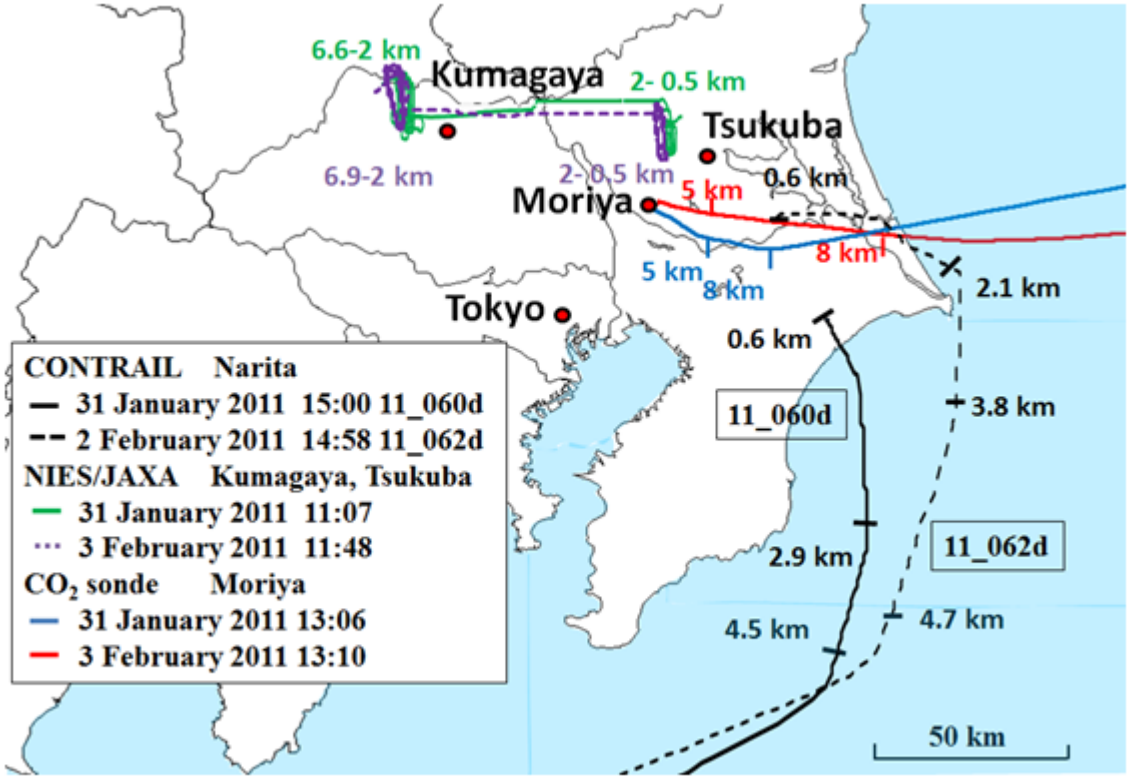

820

821

822 **Figure 6**. Flight paths of the CO_2 sonde observations launched at Moriya on January 31st (blue solid
823 line) and February 3rd (red solid line), 2011, the CONTRAIL 11_060d data on January 31st, 2011
824 (black solid line) and 11_062d data on February 2nd, 2011 (black dashed line) from Hong Kong to
825 Narita, and the NIES/JAXA chartered aircraft experiment on January 31st (green solid line) and
826 February 3rd (purple dotted line). The altitudes of the flight paths are also indicated.

827

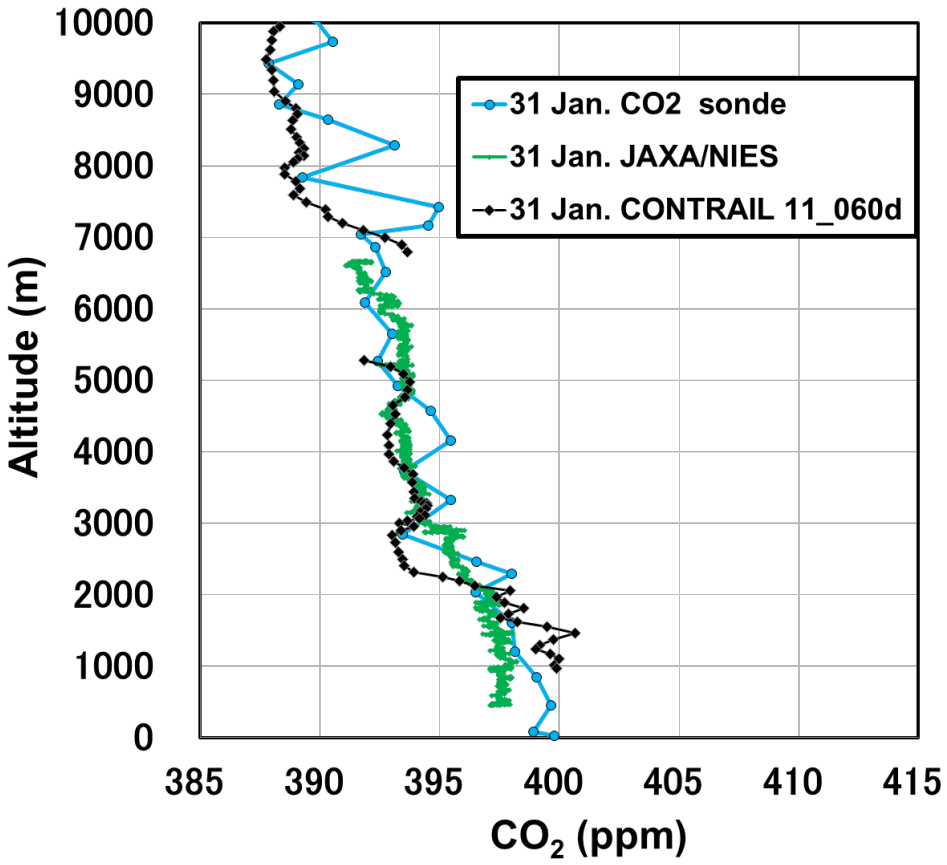

828

829 **Figure 7**. The CO_2 vertical profiles obtained by the CO_2 sonde (circles connected with blue lines),

830 NIES/JAXA chartered aircraft data (dots connected with green lines), and the CONTRAIL data

831 (diamonds connected with black lines) on January 31st, 2011.

832

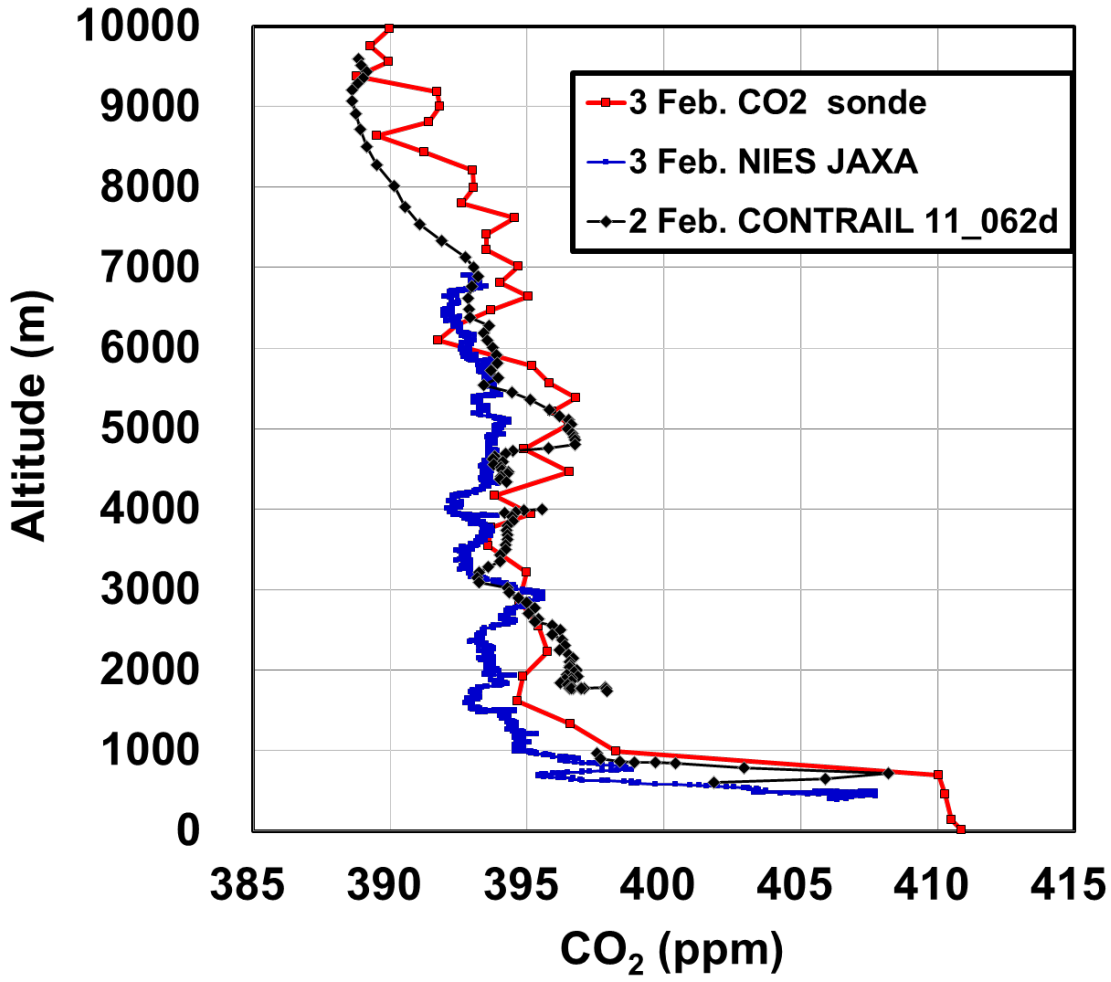

833

834

835 **Figure 8**. The CO_2 vertical profiles obtained by the CO_2 sonde (circles connected with red lines),

836 NIES/JAXA chartered aircraft data (dots connected with purple lines) on February 3rd, and

837 CONTRAIL data (diamonds connected with black lines) on February 2nd, 2011.

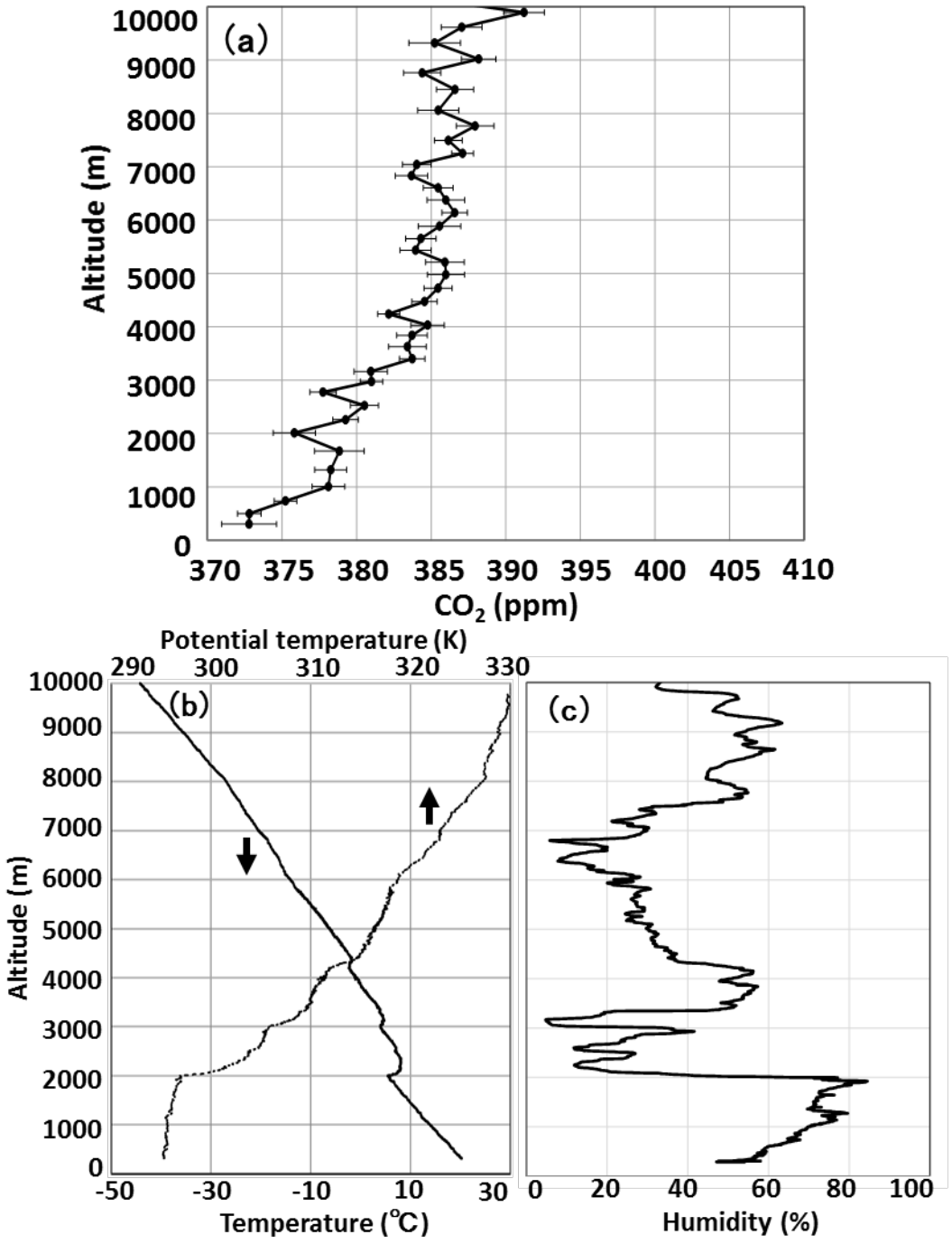

Figure 9. Profiles of (a) CO_2 mole fraction, (b) temperature (solid line) and potential temperature (dotted line), and (c) relative humidity observed over a forest area, Moshiri in Hokkaido, Japan by the balloon launched on August 26, 2009 at 13:30 (LST). The black circles with error bars in panel (a) represent the data obtained by the CO_2 sonde.

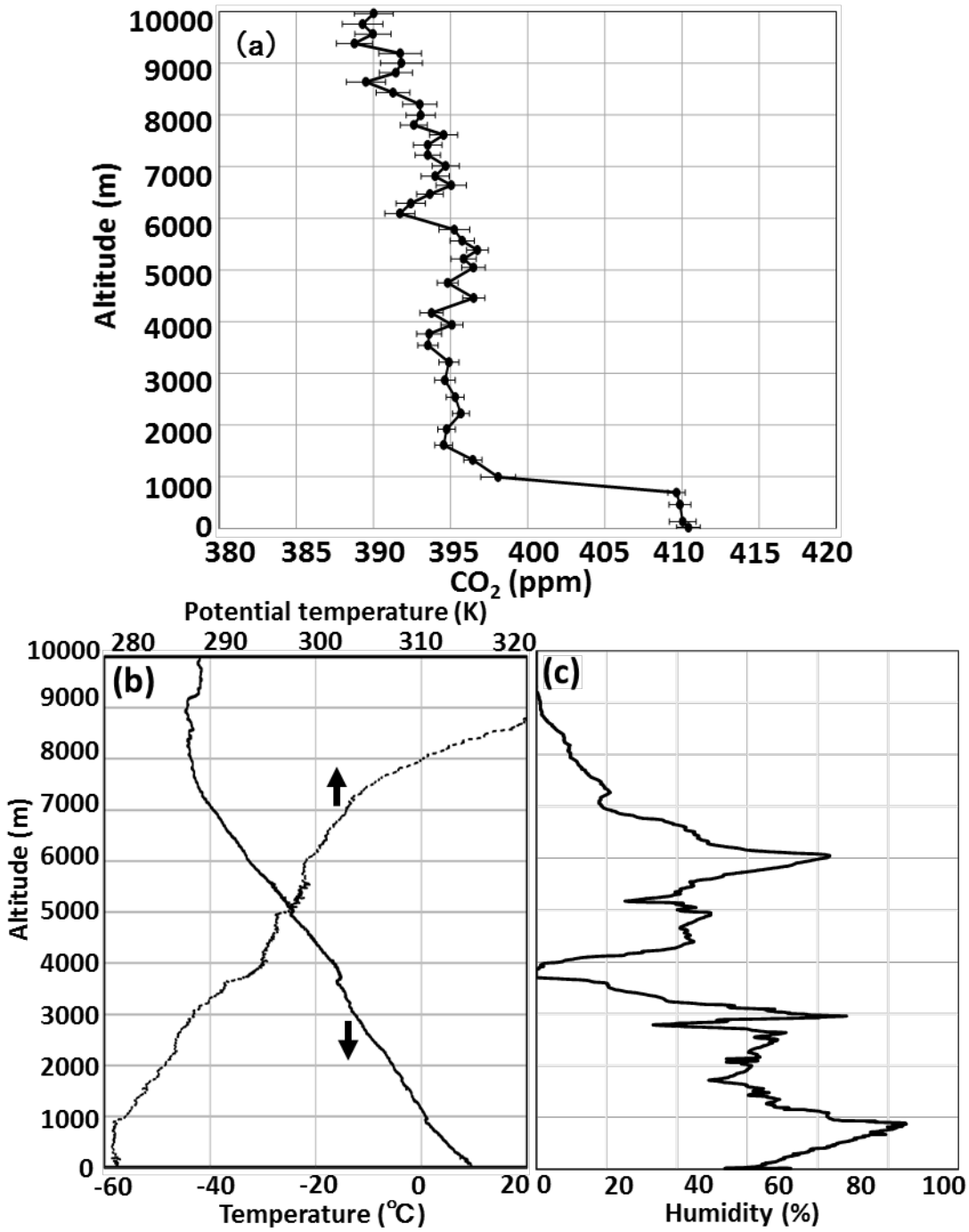

845 **Figure 10**. Profiles of (a) CO_2 mole fraction, (b) temperature (solid line) and potential temperature
846 (dotted line), and (c) relative humidity observed over an urban area, Moriya near Tokyo on February
847 3rd, 2011 at 13:10 (LST).
848